Journal of Cluster Science
https://doi.org/10.1007/s10876-021-02077-6

ORIGINAL PAPER

Cluster Modeling of Network-Forming Amorphization Pathways in As_xS_{100-x} Arsenicals ($50 \leq x \leq 57$) Diven by Nanomilling

Oleh Shpotyuk[1,2] · Malgorzata Hyla[1] · Yaroslav Shpotyuk[3,4] · Valentina Balitska[5] · Andrzej Kozdras[6] · Vitaliy Boyko[2]

Received: 26 December 2020 / Accepted: 22 April 2021

Abstract
Complete hierarchy of network amorphization scenarios initiated in As_xS_{100-x} nanoarsenicals within As_4S_4-As_4S_3 cut-Sect. ($50 \leq x \leq 57$) is reconstructed employing materials-computational approach based on ab-initio quantum-chemical modeling code (CINCA). Under nanostructurization due to high-energy mechanical milling, the inter-crystalline transformations to nanoscopic β-As_4S_4 phase accompanied by appearance of covalent-network amorphous matrix are activated. General amorphization trend under nanomilling obeys tending from molecular cage-like structures to optimally-constrained covalent-bonded networks compositionally invariant with parent arsenical. The contribution of amorphization paths in nanoarsenicals is defined by their chemistry with higher molecular-to-network barriers proper to As_4S_3-rich alloys. The generated amorphous phase is intrinsically decomposed, possessing double-T_g relaxation due to stoichiometric ($x = 40$) and non-stoichiometric ($x > 40$) sub-networks, which are built of $AsS_{3/2}$ pyramids and As-rich arrangement keeping (i) two separated As-As bonds derived from realgar-type molecules, (ii) two neighboring As-As bonds derived from pararealgar-type molecules or (iii) three neighboring As-As bonds in triangle-like geometry derived from dimorphite-type molecules. Compositional invariance of nanoamorphous phase is ensured by growing sequence of network-forming clusters with average coordination numbers Z in the row ($As_2S_{4/2}$, $Z = 2.50$) – ($As_3S_{5/2}$, $Z = 2.55$) – ($As_3S_{3/2}$, $Z = 2.67$). Diversity of main molecular-to-network amorphizing pathways in nanoarsenicals is reflected on the unified potential energy landscape specified for boundary As_4S_4 and As_4S_3 components.

Keywords Arsenicals · Amorphization · *Ab-initio* quantum-chemical modeling · Molecular cluster · Nanomilling

Introduction

The family of binary *arsenic sulphides* As_xS_{100-x} [1–6], often referred to as *arsenicals* due to their anticancer therapeutic functionality [7], are accepted as representatives of canonical substances, where diverse structure-conformation tendencies can be revealed in dependence on their chemistry. Thus, at the moderated As content in these *thioarsenide* alloys close to stoichiometry As_2S_3 (viz. $As_{40}S_{60}$), competitive matrix *amorphization* (*vitrification*) and layer-type conformation (*crystallization*) processes occur, while in As-rich As_xS_{100-x} compounds (where x exceeds 40) the latter are replaced by molecular-crystallization tendencies accompanied by stabilization of As_4S_n cage-like molecules ($n = 5,4,3$) [8–10].

Under full saturation of covalent chemical bonding in respect to the Mott's *8-N* rule [3], which is characteristic feature of many chalcogenide compounds allowing their consideration in terms of the average coordination number Z (the number of covalent bonds per atom) [5], this As-S system reveals unprecedented glass-forming ability in a vicinity of arsenic trisulphide As_2S_3 [4]. That is why the glassy g-As_2S_3 prepared by melt-quenching cannot be crystallized during prolonged thermal treatment even above glass-transition temperature T_g [2, 3], despite the known fact on existing of isocompositional mineral with layered crystalline structure (the orthorhombic orpiment possessing space group $P2_1/n$) [8]. Trigonal $AsS_{3/2}$ pyramids (as main structural motives of this glass-former) interconnected by S atoms in so-called corner- or atom-shared links form basis for under-stoichiometric covalent networks of S-rich As_xS_{100-x} arsenicals ($x < 40$), realized

Extended author information available on the last page of the article

Published online: 08 May 2021

due to polymerization (bridging) properties of $-S_n-$ chains. Therefore, the compositional domain of stable glass-formers extends in binary As-S system to $Z \sim 2.16$ dependently on melt-quenching route (it means that g-$As_{16}S_{84}$ possesses competitive S separation-agglomeration properties) [2–4]. Within this range of S-rich As_xS_{100-x} arsenicals up to stoichiometric As_2S_3 ($2.16 < Z \leq 2.40$), this system demonstrates few anomalies like *instability onsets* in cluster-forming energies [6], which were mistakenly accepted as "signatures" of intermediate optimally-constrained (rigid and stress-free) phases in covalent-bonded network substances [11].

Controversially, under enlarged As content in this As_xS_{100-x} system over As_2S_3 stoichiometry, the network-forming tendency rapidly disappears at $Z \sim 2.44$–2.46 on a cost of partially crystallized arrangement of *thioarsenide* As_4S_n molecules ($n = 5,4,3$) [1–4]. These cage-like entities (having no dangling bonds or terminated inter-cluster links) serve as main blocks for molecular crystals of some minerals, such as uzonite As_4S_5 (Z = 2.44), realgar α-As_4S_4 ($Z = 2.50$), bonazitte or β-As_4S_4 ($Z = 2.50$), pararealgar As_4S_4 ($Z = 2.50$), as well as α-/β-dimorphite As_4S_3 ($Z = 2.57$) [4, 8]. The former (the uzonite As_4S_5) along with *tetra-arsenic tetrasulphide* As_4S_4 possessing four different crystallographic polymorphs seem to be most plausible candidates for devitrification in the group of melt-quenched As_xS_{100-x} alloys at $x > 44$.

Notwithstanding, phase equilibria become more complicated with progressive increase in As content in As_xS_{100-x} arsenicals, resulting in the second glass-forming region at $51 \leq x \leq 66$. Hruby [1] was the first who considered these glasses as metastable plastic phases with T_g below room temperature. In his opinion, thermodynamically stable glasses of these compositions (with $Z = 2.51$–2.66) do not exist. The second glass-forming region in these thioarsenide alloys was shown to be superimposed with stabilization domain of *tetra-arsenic trisulphide* polymorphs As_4S_3 ($Z = 2.57$) [12, 13], meaning the crucible role of spherically-symmetric As_4S_3 cage-like molecules [14]. The plastic-crystalline rhombohedral modification of this dimorphite-type As_4S_3 phase as found by Chattopadhyay et al. [15] and further generalized by Blachnik and Wickel [16] was accepted as responsible for additional rotational disorder in these glass-formers.

This finding was further proved by Aitken for ternary $Ge_xAs_yS_{100-x-y}$ glasses with As:Ge ratio approaching ~ 17:1 [17, 18]. It was also shown [19–21] that under nanostructurization caused by external influence such as high-energy mechanical milling (nanomilling), the complicated inter-crystalline phase transformations towards nanocrystalline β-As_4S_4 polymorph (nc-β-As_4S_4) accompanied by appearance of isocompositional amorphous phase having covalent network were activated in these arsenicals along realgar-dimorphite As_4S_4–As_4S_3 cut-Sect. ($2.50 \leq Z \leq 2.57$).

In this work, the amorphization scenarios in As_xS_{100-x} arsenicals along As_4S_4-As_4S_3 line ($50 \leq x \leq 57$) will be recognized employing the advanced materials-computational approach [12, 22] developed at the basis of the authorized *ab-initio* quantum-chemical modeling code (CINCA) [6, 23, 24].

Method: the CINCA Modeling of Molecular-Network Conformations in Covalent Substances

The geometrically-optimized configurations of As_4S_n cage-like molecules (n = 4,3) and their network-forming derivatives responsible for amorphization in As_xS_{100-x} arsenicals along As_4S_4-As_4S_3 cut-line were simulated with *ab-initio* quantum-chemical cluster-modeling algorithm CINCA (cation-interlinked network cluster approach) [6, 23, 24]. Network-forming clusters were reconstructed by breaking respective As_4S_4 or As_4S_3 molecules on distinct fragments linking them with surrounding matrix by $S_{1/2}…S_{1/2}$ bridging chains. The HyperChem Release 7.5 program package based on restricted Hartree–Fock self-consistent field method with split-valence double-zeta basis set and single polarization function 6-311G* [25–27] was employed for cluster energy calculations. Final geometrical optimization and single-point energy calculations for selected clusters were performed employing the Fletcher-Reeves conjugate gradient method until the root-mean-square gradient of 0.1 kcal/(Å·mol) was reached. The calculated cluster-forming energies E_f were corrected on the energy of terminated H atoms used to transform the network-forming clusters into molecular self-consistent precursors according to the procedure developed elsewhere [27, 28], and finally determined in respect to the energy of single trigonal $AsS_{3/2}$ pyramid ($E_f = -79.404$ kcal/mol) [6, 23].

Thus, the developed cluster-modeling code CINCA allows quantitative comparison between molecular- and network-forming tendencies in covalent substances, parameterizing adequately competitive crystallization-amorphization scenarios.

Results and Discussion

Cluster Modeling of Amophization Paths Derived from Realgar-Type α/β-As_4S_4 Polymorphs

The quantum-chemical model of realgar-type As_4S_4 molecule (see Fig. 1a) was developed in our preliminary

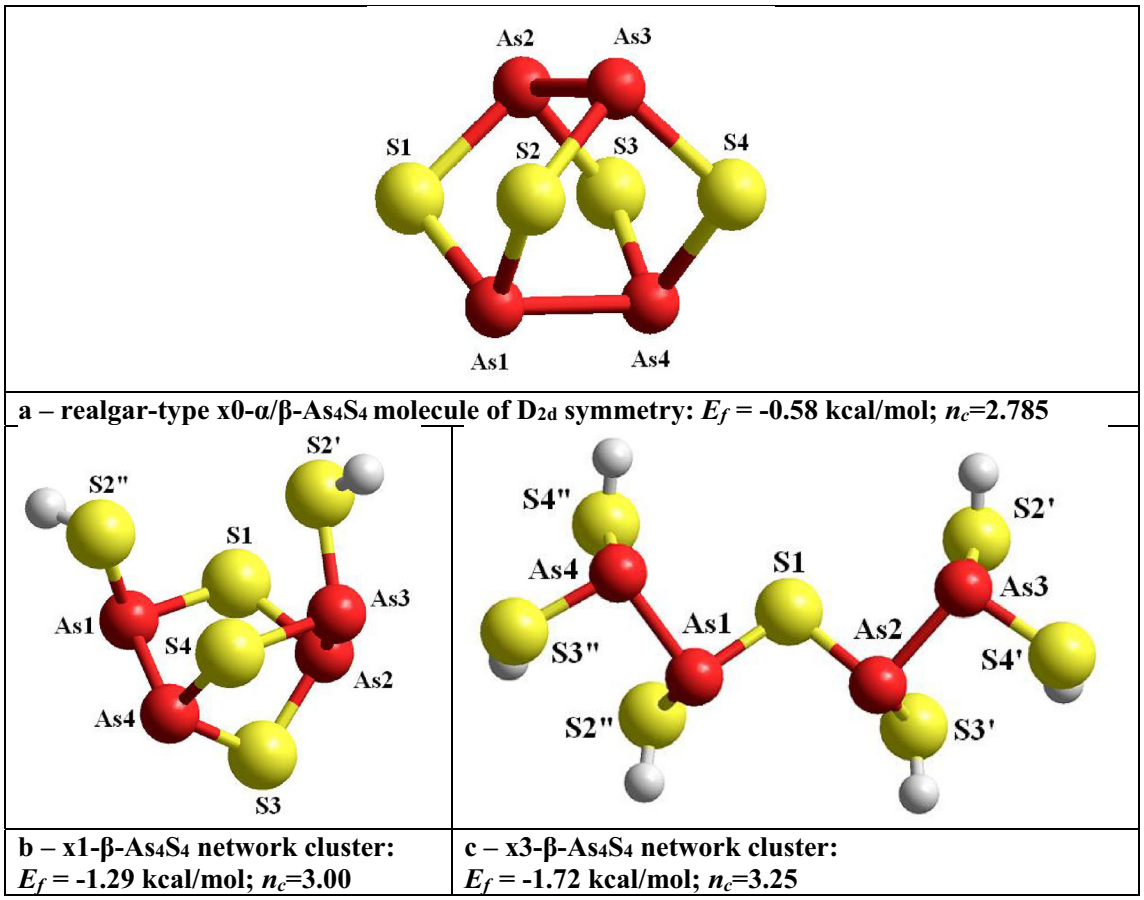

Fig. 1 Geometrically-optimized configurations of realgar-type α/β-As_4S_4 cage-like molecule (**a**) and its energetically favorable network derivatives formed from $As_4S_5H_2$ molecule by single × 1-break in S1 position (**b**), and from $As_4S_7H_6$ molecule by triple × 3-break in S1-S2-S3 positions (**c**). The terminated H atoms are grey-colored, S and As atoms are yellow- and red-depicted, and covalent bonds between atoms are denoted by respectively colored sticks [19, 22]

research [29]. This cage-like molecule of D_{2d} symmetry built of 8 heteronuclear As-S bonds and 2 homonuclear As-As bonds in separated mutually orthogonal configuration evolves 8 small rings (4 pentagons and 4 hexagons), thus resulting in under-constrained structural motive possessing average number of topological constraints per atom n_c = 2.875 (in respect to the Phillips-Thorpe constraint-counting algorithm [30–32] applied to stretching and bending forces ascribed to bonds in this molecule). The same symmetric As_4S_4 molecule (with intramolecular bond lengths and angles close to those refined from realistic crystalline structures) is character for mineral realgar α-As_4S_4 [33, 34], synthetic β-As_4S_4 [35] and its natural analogue (mineral bonazziite As_4S_4 [36]). The calculated cluster-forming energy E_f for this molecule (in respect to the energy of $AsS_{3/2}$ pyramid) equals − 0.58 kcal/mol (Table 1) [19, 22], the value dominated over all molecular and network-forming arsenical clusters within compositional range of interest ($2.50 \leq Z \leq 2.57$).

The most plausible amorphization scenarios in arsenic monosulphide AsS (viz. As_4S_4) are related to high-temperature *tetra-arsenic tetrasulphide* β-As_4S_4 polymorph [10, 19, 20]. This specificity is revealed due to lower barrier of α-As_4S_4-to-β-As_4S_4 transition [37] as compared with nanostructurization-driven amorphization from each of these phases (low-temperature α-As_4S_4 or high-temperature β-As_4S_4), provided direct low-to-high-temperature phase transformation was not inhibited.

Among a group of network-forming derivatives from this realgar-type cage-like molecule (β-As_4S_4), the smallest cluster-forming energy $E_f = -1.29$ kcal/mol is achieved for single-broken × 1-β-As_4S_4 cluster (see Table 1) derived from $As_4S_5H_2$ molecular precursor as shown on Fig. 1b [19, 22]. This cluster having one hexagon and two pentagons in atomic arrangement is optimally-constrained since $n_c = 3.00$, which is in strict respect to space dimensionality ($D = 3$). Therefore, covalent-bonded structures bult of such clusters are most favorable for amorphization. Because of low barrier with ground state of As_4S_4 molecule due to ΔE_f = (1.29–0.58) kcal/mol = 0.71 kcal/mol, the expected molecular-to-network transformation occurs even in directly synthesized arsenic monosulphide, being a

Table 1 Cluster-forming energies E_f (in respect to the energy of $AsS_{3/2}$ pyramid) for network-forming derivatives from realgar-type β-As_4S_4 molecule (atomic labels refer to Fig. 1a) [19, 22]

Molecular prototype	Network/molecular cluster, and respective cluster-forming scenario	Number of rings: hexagons/pentagons	n_c	E_f, (kcal/mol)
β-As_4S_4	no break (× 0-break)	4/4	2.875	− 0.58
$As_4S_5H_2$	× 1-β-As_4S_4, × 1-break in S1	1/2	3.00	− 1.29
$As_4S_6H_4$	× 2–1-β-As_4S_4, × 2-break in S1-S3	0/1	3.125	− 3.47
$As_4S_6H_4$	× 2–2-β-As_4S_4, × 2-break in S1-S4	1/0	3.25	− 12.59
$As_4S_7H_6$	× 3-β-As_4S_4, × 3-break in S1-S2-S3	0/0	3.25	− 1.72
$As_4S_8H_8$	× 4-β-As_4S_4, × 4-break in S1-S2-S3-S4	0/0	3.25	− 1.72

source of uncontrolled spontaneous amorphization [10, 19, 38–40].

An alternative path of induced amorphization in β-As_4S_4 is related to × 3-β-As_4S_4 network-forming cluster prototyped by $As_4S_7H_6$ molecule which appears as triple-broken derivative from realgar-type As_4S_4 molecule possessing chain structure without small rings (see Fig. 1c) [19, 22]. Despite evidently over-constrained constitution (in view of n_c = 3.25), the small E_f value approaching − 1.72 kcal/mol is character for this cluster (see Table 1), resulting in low molecular-to-network barrier ΔE_f = 1.14 kcal/mol [19]. This cluster is commensurable (within ± 0.03 kcal/mol error-bar proper to CINCA calculations [23]) with other one, the quadruple-broken × 4-β-As_4S_4 (or, alternatively, $As_2S_{4/2}$ cluster) obtained by breaking in all S atom positions, thus keeping separated As-As bond in network. These × 3-β-As_4S_4 clusters surely dominate in nanostructured arsenicals (nanoarsenicals) in view of lower number of covalent bonds destructed in × 0-β-As_4S_4 molecule.

Thus, full variety of amorphization scenarios derived from β-As_4S_4 phase can be depicted on potential energy landscape as shown on Fig. 2. The above network-forming derivatives (× 1-β-As_4S_4 and × 3-β-As_4S_4) evidently prefer over other variants of network clustering originated in part due to double-breaking of covalent bonds in realgar-type As_4S_4 molecule (× 2–1-β-As_4S_4 and × 2–2-β-As_4S_4) [19].

Cluster Modeling of Amorphization Scenarios Activated from Pararealgar As_4S_4 Phase

Pararealgar As_4S_4 as metastable product of light-induced alteration from both tetra-arsenic tetrasulphide polymorphs (α-As_4S_4 and β-As_4S_4) [8, 41, 42], was found to exist (albeit in small amount) in As_4S_4-As_4S_3 alloys prepared by melt-quenching and/or nanomilling [20] (following the Kyono's notation [43], and for sake of convenience, this phase will be marked thereafter as p-As_4S_4). Notwithstanding, the network-forming tendencies derived from this pararealgar p-As_4S_4 phase should be accepted in the overall balance of possible amorphization scenarios in the studied arsenicals, provided they were preliminary light-soaked.

The simulated pararealgar-type p-As_4S_4 cage-like molecule possesses reduced C_s symmetry due to asymmetric adjacent configuration of two neighboring homonuclear As-As bonds (such as As4-As3 and As2–As3 on Fig. 3a) with common As3 atom, the optimized parameters of this configuration in Table 2 being agreed with those determined from the known experimental model [40]. This p-As_4S_4 molecule includes one tetragon (As2As3As4S1), two pentagons (As1S2As2As3S3 and As1S4As4As3S3) and one hexagon (As1S4As4S1As2S2), thus resulting in under-constrained topological motive with n_c = 2.75 (Table 3). In comparison with realgar-type As_4S_4 molecule (Fig. 1a), the calculated E_f energy for this molecule is higher approaching − 0.94 kcal/mol.

A great variety of network-forming clusters are expected from this asymmetric configuration of metastable p-As_4S_4 molecule, their small-ring characteristics (number and type of small rings, hexagons/pentagons/tetragons) and cluster-forming energies E_f being presented in Table 3. The most plausible among them seems to be × 4-p-As_4S_4 cluster reconstructed from $As_4S_8H_8$ molecular precursor due to quadruple × 4-break in all S atom positions, which completely destroys small-ring structure of this molecule separating arsenical matrix on AsS_3H_3 and $As_3S_5H_5$ molecular precursors (see Fig. 3b). From network-reconstruction viewpoint, this cluster with equivalent bond distances and angles given in Table 4 results in over-constrained topology of overall backbone with n_c = 3.25 in average. Realistically, this configuration split into amorphous subnetworks composed of optimally-constrained interlinked $AsS_{3/2}$ pyramids (Z = 2.40; n_c = 3.00) and over-constrained stressed-rigid $As_3S_{5/2}$ chains (Z = 2.55; n_c = 3.36). Direct bonded As–S and As–As distances in these clusters fit respectively within ∼ 2.26 Å and ∼ 2.47 Å, while

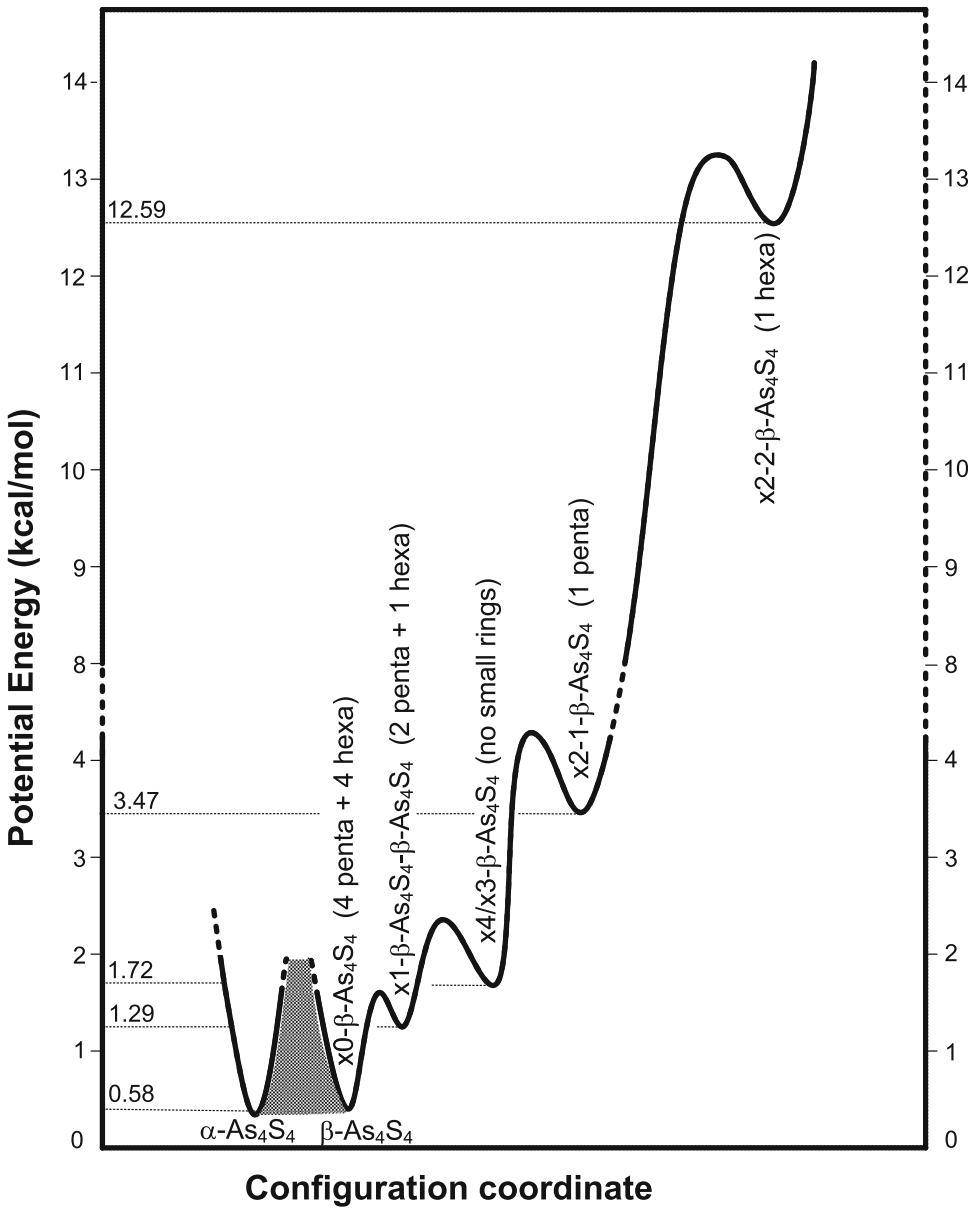

Fig. 2 Potential energy landscape showing amorphization scenarios derived from β-As_4S_4 phase. The settle-points corresponding to network clusters derived from realgar-type As_4S_4 molecules by *x*-fold bond-breaking (keeping small rings, such as pentagons/hexagons nominated in parenthesis) are denoted with respective cluster-forming energies E_f at the right axis. The ground molecular-crystalline state is given in double-well presentation for low-temperature realgar α-As_4S_4 and high-temperature β-As_4S_4 polymorph (no amorphization transitions are expected from α-As_4S_4 state)

more essential deviations are observed in bond angles at As atoms. Molecular-to-network barrier for this amorphization pathway is low approaching ΔE_f = (1.56–0.94) kcal/-mol = 0.62 kcal/mol, this value being comparable with ΔE_f for other transitions forming optimally-constrained single-broken × 1–1-p-As_4S_4 (ΔE_f = 0.84 kcal/mol) and triple-broken × 3–1-p-As_4S_4 derivatives (ΔE_f = 1.19 kcal/mol) having n_c = 3.00, along with over-constrained double-broken × 2–4-p-As_4S_4 derivatives with n_c = 3.25 (ΔE_f = 1.15 kcal/mol). These data testify in favor of rather shallow-level character of respective potential energy landscape on Fig. 4 illustrating amorphization scenarios originated from pararealgar-type p-As_4S_4 arsenicals. Because of low barriers between these wells, transition towards quadruple-broken × 4-p-As_4S_4 network-forming clusters possessing E_f = − 1.56 kcal/mol seems to be most favorable.

Thus, decomposition on two different topological sub-networks occurs first from p-As_4S_4 arsenical, these being *stoichiometric* optimally-constrained (Z = 2.40, n_c = 3.00) and *non-stoichiometric* As-rich over-constrained ones (Z = 2.55, n_c = 3.36). In the realistic arsenical systems compositionally close to arsenic monosulphide AsS, this process is expected to be merely blocked, provided appearance of pararealgar p-As_4S_4 phase is inhibited.

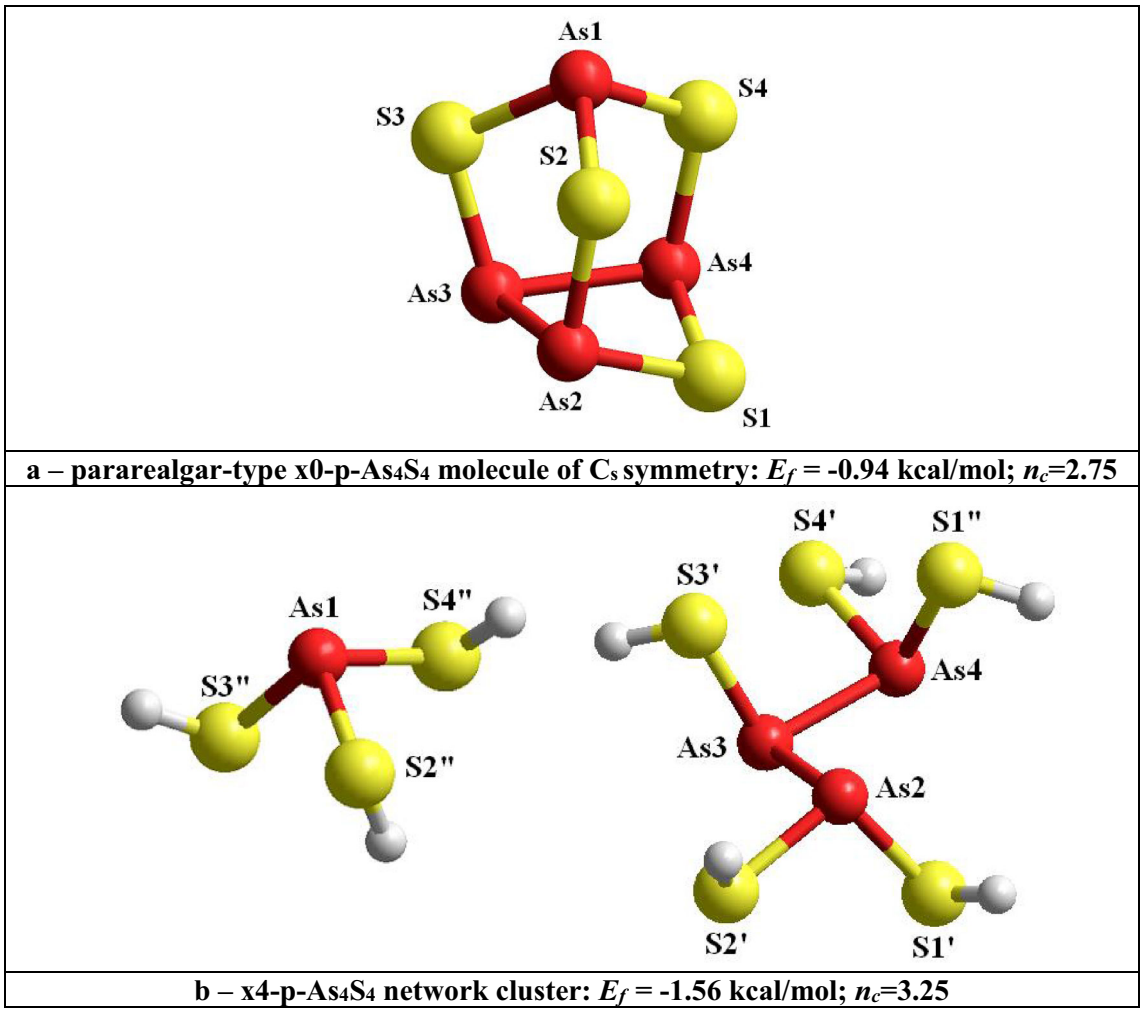

Fig. 3 Geometrically-optimized configurations of pararealgar-type p-As_4S_4 cage-like molecule (**a**) and its most energetically favorable network derivative separating arsenical matrix on AsS_3H_3 and $As_3S_5H_5$ molecules due to quadruple × 4-break in S1-S2-S3-S4 positions. The terminated H atoms are grey colored, S and As atoms are respectively depicted by yellow and red balls, and covalent bonds between atoms are stick-denoted

Cluster Modeling of Amorphization Paths Derived from Dimorphite α/β-As_4S_3 Phases

Removing one S atom at the bottom of pararealgar p-As_4S_4 molecule (within As2-As3-As4-S1 sequence, Fig. 3a), replacing it by one As-As bond, transfers this molecule to other one As_4S_3-I corresponding to both low- and high-temperature polymorphs of mineral dimorphite α/β-As_4S_3 [12, 13]. This is most energetically plausible configuration of this As_4S_3 molecule formed from six heteronuclear As-S and three homonuclear As–As bonds as shown on Fig. 5a. The optimized bond distances and angles in this × 0-As_4S_3-I molecule obeying *triangle-like* conformation due to the basal 3-membered As_3-ring (triangle) composed of As2–As3–As4 atoms, surmounted by $AsS_{3/2}$ pyramid composed of As1–(S1–S2–S3) atoms (see Fig. 5a) have been derived from CINCA modeling and gathered in Table 5. It's seen that direct bonded As-As distances in As_3-triangle approach ∼ 2.467 Å with all bond angles close to ∼ 60°. Direct bonded As-S distances within $AsS_{3/2}$ pyramid and As-S distances connecting this pyramid with bottom As_3-ring approach ∼ 2.235 Å, with angle on As1 atom at the apex of $AsS_{3/2}$ pyramid close to ∼ 99.04°. The calculated E_f energy for this molecule (in respect to the energy of $AsS_{3/2}$ pyramid) was found to be − 1.78 kcal/mol (see Table 6), the value worse than in molecular As_4S_4-type polymorphs, but comparable and even better than in network-forming derivatives from these cage-like molecules (compare respective energies in Tables 1, 3, 6).

Previously, the crystallographic features of under-constrained As_4S_3 molecule (n_c = 2.71, Table 6) possessing C_{3v} symmetry with four small rings (three pentagons and one triangle) were specified (see, e.g. refs. [8, 14]), and geometrically-optimized parameters of this molecule were

Table 2 Geometrically-optimized bond distances and angles in parareal gar-type p-As_4S_4 molecule (atom labels refer to Fig. 3a)

Equivalent bond distances				Equivalent bond angles	
Atoms	Distance (Å)	Atoms	Distance (Å)	Angle	Deg. (°)
Direct bonded distances				∠ *S–As–S*	
As3–As4	2.4898	As2–As3	2.4905	∠ S1–As4–S4	104.406
As1–S2	2.2453	As2–S1	2.2652	∠ S1–As2–S2	104.398
As1–S3	2.2486	As2–S2	2.2487	∠ S2–As1–S4	104.239
As1–S4	2.2460	As4–S1	2.2652	∠ S2–As1–S3	98.843
As3–S3	2.2141	As4–S4	2.2486	∠ S3–As1–S4	98.783
Non–bonded distances				∠ *S–As–As*	
As1–As2	3.6481	As1–As4	3.6487	∠ S3–As3–As2	101.756
As1–As3	3.4837	As2–As4	3.3508	∠ S3–As3–As4	101.754
				∠ S2–As2–As3	100.465
As1–S1	4.3673	As3–S2	3.6460	∠ S4–As4–As3	100.457
As2–S3	3.6540	As3–S4	3.6452	∠ S1–As2–As3	86.002
As2–S4	4.1150	As4–S2	4.1154	∠ S1–As4–As3	86.019
As3–S1	3.2476	As4–S3	3.6533	∠ *As–As–As*	
				∠ As2–As3–As4	84.570
S1–S2	3.5668	S2–S3	3.4132	∠ *As–S–As*	
S1–S3	4.7549	S2–S4	3.5449	∠ As2–S2–As1	108.539
S1–S4	3.5666	S3–S4	3.4122	∠ As4–S4–As1	108.543
				∠ As3–S3–As1	102.635
				∠ As2–S1–As4	95.398

Table 3 Cluster-forming energies E_f (in respect to the energy of $AsS_{3/2}$ pyramid) for network-forming derivatives from parareal gar-type p-As_4S_4 molecule (atom labels refer to Fig. 3a)

Molecular prototype	Network/molecular cluster, and respective cluster-forming path	Number of rings: hexagons/pentagons/tetragons	n_c	E_f, (kcal/mol)
p-As_4S_4	× 0-p-As_4S_4, no break (× 0-break)	1/2/1	2.75	− 0.94
$As_4S_5H_2$	× 1–1-p-As_4S_4, × 1-break in S1	0/2/0	3.00	− 1.78
$As_4S_5H_2$	× 1–2-p-As_4S_4, × 1-break in S2	0/1/1	2.875	− 3.01
$As_4S_5H_2$	× 1–3-p-As_4S_4, × 1-break in S3	1/0/1	3.00	− 3.09
$As_4S_6H_4$	× 2–1-p-As_4S_4, × 2-break in S2–S4	0/0/1	3.00	− 4.82
$As_4S_6H_4$	× 2–2-p-As_4S_4, × 2-break in S2–S1	0/1/0	3.125	− 8.41
$As_4S_6H_4$	× 2–3-p-As_4S_4, × 2-break in S2–S3	0/0/1	3.00	− 12.12
$As_4S_6H_4$	× 2–4-p-As_4S_4, × 2-break in S3–S1	1/0/0	3.25	− 2.09
$As_4S_7H_6$	× 3–1-p-As_4S_4, × 3-break in S2–S4–S3	0/0/1	3.00	− 2.13
$As_4S_7H_6$	× 3–2-p-As_4S_4, × 3-break in S2–S4–S1	0/0/0	3.25	− 7.98
$As_4S_7H_6$	× 3–3-p-As_4S_4, × 3-break in S2–S3–S1	0/0/0	3.25	− 7.14
$As_4S_8H_8$	× 4-p-As_4S_4, × 4-break in S1–S2–S3–S4	0/0/0	3.25	− 1.56

derived from *ab-initio* quantum-chemical model of Kyono [43]. However, the energetic specificity of competitive molecular-network amorphizing tendencies in dimorphite-type As_4S_3 arsenicals has not been established.

In general, dimorphite α/β-As_4S_3-type molecule allows three network-forming configurations, which can be reconstructed from × 0-As_4S_3-I cages shown on Fig. 5a by × 1-, × 2-, × 3-breaking in respective S1, S2, S3 positions, these configurations being parameterized and compared in Table 6.

The optimally-constrained double-broken × 2-As_4S_3-I clusters having n_c = 3.00 in view of one small ring kept in the structure (As_3-triangle) cannot be stabilized in realistic amorphous structures because of unfavorable cluster-

Table 4 Geometrically-optimized bond distances and angles in network derivative from pararealgar-type p-As_4S_4 cage-like molecule separating matrix on AsS_3H_3 and $As_3S_5H_5$ molecules due to quadruple × 4-break in all S atoms (atom labels refer to Fig. 3b)

Equivalent bond distances				Equivalent bond angles	
Atoms	Distance (Å)	Atoms	Distance (Å)	Angle	Deg. (°)
AsS_3H_3 molecule					
Direct bonded distances				∠ *S–As–S*	
As1–S2″	2.2540	As1–S4″	2.2561	∠ S4″–As1–S2″	101.939
As1–S3″	2.2515			∠ S4″–As1–S3″	92.673
Non-bonded distances				∠ S2″–As1–S3″	102.941
S2″–S3″	3.5246	S3″–S4″	3.2608		
S2″–S4″	3.5035				
$As_3S_5H_5$ molecule					
Direct bonded distances				∠ *S–As–S*	
As3–As4	2.4730	As2–As3	2.4659	∠ S1″–As4–S4′	101.787
As2–S1′	2.2605	As4–S1″	2.2595	∠ S1′–As2–S2′	101.412
As2–S2′	2.2611	As4–S4′	2.2525	∠ *S–As–As*	
As3–S3′	2.2573			∠ S1′–As2–As3	94.938
Non-bonded distances				∠ S2′–As2–As3	95.462
As2–As4	3.7602	S1′–S1″	4.7220	∠ S3′–As3–As2	94.414
As2–S1″	3.9534	S1′–S2′	3.4992	∠ S3′–As3–As4	102.986
As2–S3′	3.4688	S1′–S3′	5.3008	∠ S1″–As4–As3	103.109
As2–S4′	5.4982	S1′–S4′	6.0459	∠ S4′–As4–As3	94.737
As3–S1′	3.4856	S2′–S1″	6.0918	∠ *As–As–As*	
As3–S1″	3.7089	S2′–S3′	4.2681	∠ As2–As3–As4	99.165
As3–S2′	3.5006	S2′–S4′	6.9640		
As3–S4′	3.4799	S3′–S1″	3.8688		
As4–S1′	3.9519	S3′–S4′	3.8463		
As4–S2′	5.5827	S4′–S1″	3.5012		
As4–S3′	3.7041				

forming energy $E_f = -11.68$ kcal/mol (Table 6). The most plausible amorphization path originated from this α/β-As_4S_3-type arsenical seems to be related to other possibility of molecular-cage destroying connected with × 3-break in all S atom positions, when arsenical matrix built of × 3-As_4S_3-I clusters ($Z = 2.57$; $n_c = 3.00$) are decomposed in two optimally-constrained sub-networks having AsS_3H_3 and $As_3S_3H_3$ molecular precursors (Fig. 5c). Like in pararealgar structures, one sub-network is composed of $AsS_{3/2}$ pyramids ($Z = 2.40$; $n_c = 3.00$) with identical parameters (compare these parameters for AsS_3H_3 molecule separated from p-As_4S_4 in Table 4 and from α/β-As_4S_3 in Table 7). Other sub-network decomposed from dimorphite-type arsenicals under × 3-break represents optimally-constrained $As_3S_{3/2}$ clusters ($Z = 2.67$; $n_c = 3.00$) keeping basal As_3-ring incorporated by triplicate = As–S– chain links. As it follows from potential energy landscape on Fig. 6a, the calculated molecular-to-network barrier for this amorphization path is low ΔE_f = (3.96–1.78) kcal/mol = 2.18 kcal/mol. The only competitive variant for this amorphization scenario in dimorphite-type arsenicals is incomplete destroying of As_4S_3-I molecule in *triangle-like* conformation due to × 1-break in S1 position keeping two neighboring small rings (triangle As2As3As4 and pentagon As2As4S3As1S1, see Fig. 5b), thus stabilizing under-constrained amorphous matrix with $n_c = 2.86$ and comparable value of $E_f = -4.24$ kcal/mol.

The *triangle-like* conformation shown in Fig. 5a is not alone arrangement of As_4S_3 molecular cages, two other under-constrained configurations, the *chain-like* As_4S_3-II with $n_c = 2.71$ (Fig. 7a) and *star-like* As_4S_3-III with $n_c = 2.57$ (Fig. 8a), being also possible. The optimized geometrical parameters for these molecules were simulated by Kyono [43], however, this author was failed to distinguish energetically realistic configurations among these As_4S_3-type arsenicals.

Removing S atom from one of two equivalent positions S2 or S4 within asymmetric p-As_4S_4 molecule on Fig. 3a, replacing it by As-As bond, transfers this molecule to other one As_4S_3-II distinguished by *chain-like* or *zig–zag* conformation due to sequent arrangement of all four As atoms (within As1As3As2As4 chain as shown in Fig. 7a). The cluster-forming E_f energies for geometrically-optimized configuration of this molecule and its main network-

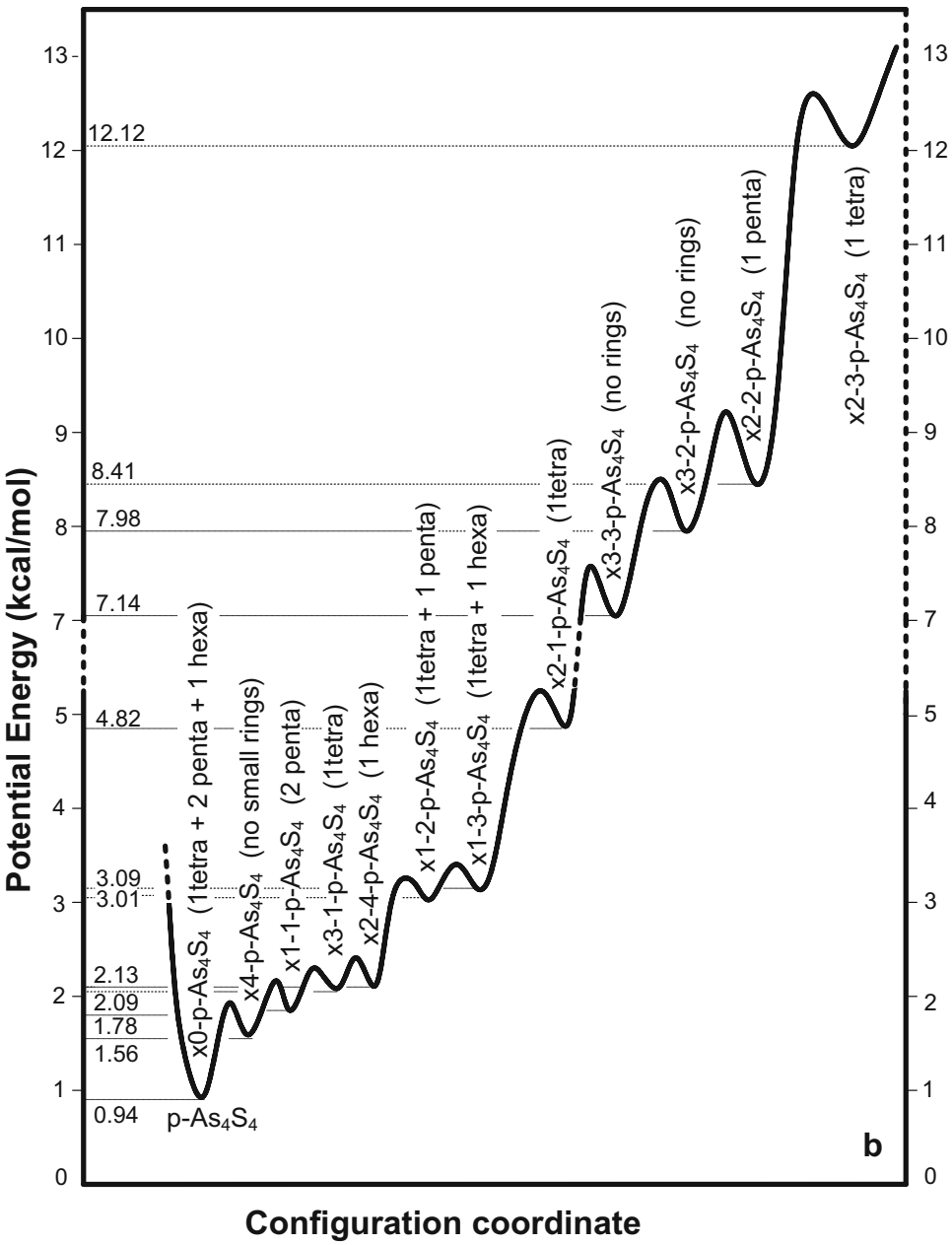

Fig. 4 Potential energy landscape illustrating amorphization scenarios derived from pararealgar-type p-As_4S_4 arsenical. The shallow-level character of network-forming derivatives reconstructed from pararealgar × 0-p-As_4S_4 molecule is obvious. The settle-points of network clusters derived by *x*-fold bond-breaking (keeping small rings, such as tetragons/pentagons/hexagons nominated in parenthesis) are denoted with respective cluster-forming energies E_f at the right axis

forming derivatives are gathered in Table 6 and reflected on potential energy landscape (see Fig. 6b). It's clearly seen that two types of network derivatives (single-broken × 1–1–As_4S_3-II with n_c = 3.00 and triple-broken × 3-As_4S_3-II with n_c = 3.43) are more favorable than parent × 0-As_4S_3-II molecule, the configuration of optimally-constrained × 1–1-As_4S_3-II network cluster being shown on Fig. 7b. It means that this *chain-like* molecular conformation cannot be stabilized realistically, being rather defective one.

The similar finding concerns other conformation possible for molecular As_4S_3 cages on Fig. 8a. This is so-called *star-like* conformation of × 0-As_4S_3-III molecule, which can be reconstructed from pararealgar p-As_4S_4 molecule (Fig. 3a) removing S atom from S3 position of surmounted pyramid As1(S2S3S4). The character *star-like* configuration in this molecule is formed by central As4 atom bonded to other three As atoms (As1, As2, and As3) as illustrated on Fig. 8a. As it follows from potential energy landscape on Fig. 6c, this under-constrained × 0-As_4S_3-III molecule (n_c = 2.57) is evidently unfavorable before two over-constrained network derivatives such as double-broken × 2-As_4S_3-III with n_c = 3.14 (Fig. 8b) and triple-broken × 3-As_4S_3-III with n_c = 3.43. Therefore, as in the previous case, the *star-like* conformation is not expected in realistic As_4S_3-type arsenical structures.

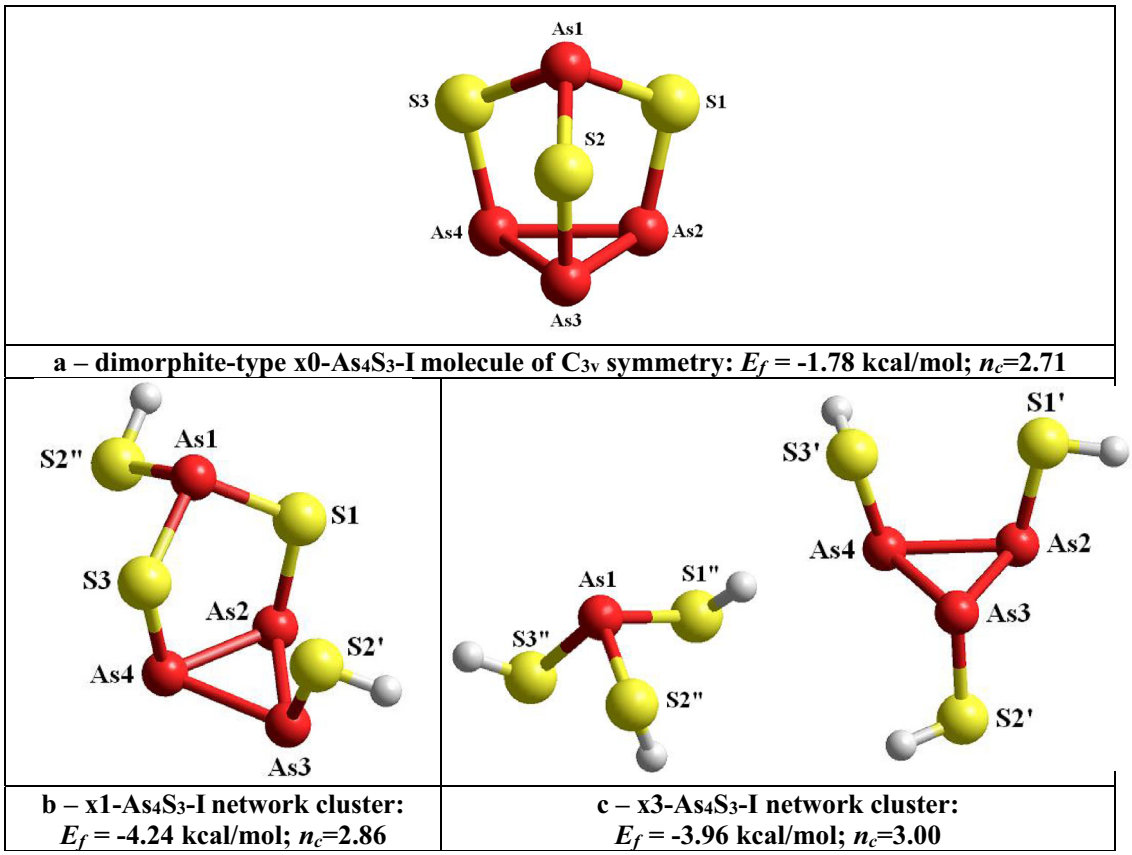

Fig. 5 Geometrically-optimized configurations of dimorphite-type α/β-As_4S_3 cage-like molecule in *triangle-like* conformation × 0-As_4S_3-I (**a**) and its most energetically favorable network derivatives formed from $As_4S_4H_2$ molecule by single × 1-break in S2 position (**b**) and separating matrix on AsS_3H_3 and $As_3S_3H_3$ molecules due to triple × 3-break in S1-S2-S3 positions (**c**). The terminated H atoms are grey-colored, S and As atoms are yellow- and red-depicted, and covalent bonds between atoms are stick-denoted

Table 5 Geometrically-optimized bond distances and angles in dimorphite-type α/β-As_4S_3 cage-like molecule (atom labels refer to Fig. 5a)

Equivalent bond distances				Equivalent bond angles			
Atoms	Distance (Å)	Atoms	Distance (Å)	Angle	Deg. (°)	Angle	Deg. (°)
Direct bonded distances				∠ *S–As–S*		∠ *As–S–As*	
As2–As3	2.4668	As3–As4	2.4664	∠ S1–As1–S2	99.042	∠ As1–S1–As2	104.627
As2–As4	2.4668			∠ S1–As1–S3	99.040	∠ As1–S2–As3	104.596
As1–S1	2.2349	As2–S1	2.2348	∠ S2–As1–S3	99.037	∠ As1–S3–As4	104.595
As1–S2	2.2353	As3–S2	2.2349				
As1–S3	2.2352	As4–S3	2.2349	∠ *S–As–As*		∠ *As–As–As*	
Non-bonded distances				∠ S1–As2–As3	102.039	∠ As3–As2–As4	59.990
As1–As2	3.5372	As1–As4	3.5368	∠ S1–As2–As4	102.038	∠ As2–As3–As4	60.005
As1–As3	3.5368	As4–S1	3.6577	∠ S2–As3–As2	102.069	∠ As2–As4–As3	60.005
As2–S2	3.6586	As4–S2	3.6580	∠ S2–As3–As4	102.058		
As2–S3	3.6586	S1–S2	3.4002	∠ S3–As4–As2	102.068		
As3–S1	3.6577	S1–S3	3.4001	∠ S3–As4–As3	102.062		
As3–S3	3.6581	S2–S3	3.4003				

Table 6 Cluster-forming energies E_f (in respect to the energy of $AsS_{3/2}$ pyramid) for network-forming derivatives from As_4S_3-type cage-like molecules (atom labels refer to Fig. 5a, 7a, 8a)

Molecular prototype	Network/molecular cluster, and respective cluster-forming path	Number of rings: pentagons/tetragons/triangles	n_c	E_f (kcal/mol)
Dimorphite-type α/β-As_4S_3 cage-like molecule in *triangle-like* conformation				
As_4S_3-I	× 0-As_4S_3-I, no breaks	3/0/1	2.71	− 1.78
$As_4S_4H_2$	× 1-As_4S_3-I, × 1-break in S1	1/0/1	2.86	− 4.24
$As_4S_5H_4$	× 2-As_4S_3-I, × 2-break in S1–S2	0/0/1	3.00	− 11.68
$As_4S_6H_6$	× 3-As_4S_3-I, × 3-break in S1–S2–S3	0/0/1	3.00	− 3.96
As_4S_3 cage-like molecule in *chain-like* conformation				
As_4S_3-II	× 0-As_4S_3-II, no breaks	2/2/0	2.71	− 3.23
$As_4S_4H_2$	× 1–1-As_4S_3-II, × 1-break in S2	1/1/0	3.00	− 3.11
$As_4S_4H_2$	× 1–2-As_4S_3-II, × 1-break in S1	0/2/0	2.86	− 5.02
$As_4S_5H_4$	× 2–1-As_4S_3-I, × 2-break in S2–S3	1/0/0	3.29	− 13.60
$As_4S_5H_4$	× 2–2-As_4S_3-I, × 2-break in S1–S3	0/1/0	3.14	− 8.30
$As_4S_6H_6$	× 3-As_4S_3-II, × 3-break in S1–S2–S3	0/0/0	3.43	− 3.17
As_4S_3 cage-like molecule in *star*-like conformation				
As_4S_3-III	× 0-As_4S_3-III, no breaks	0/3/0	2.86	− 4.66
$As_4S_4H_2$	× 1-As_4S_3-III, × 1-break in S1	0/2/0	2.86	− 5.41
$As_4S_5H_4$	× 2-As_4S_3-III, × 2-break in S1–S2	0/1/0	3.14	− 3.11
$As_4S_6H_6$	× 3-As_4S_3-III, × 3-break in S1–S2–S3	0/0/0	3.43	− 3.55

Table 7 Geometrically-optimized bond distances and angles in network derivative from dimorphite α/β-As_4S_3 cage-like molecule in *triangle-like* conformation, separating matrix on AsS_3H_3 and $As_3S_3H_3$ molecules due to triple × 3-break in S1-S2-S3 positions (atom labels refer to Fig. 5c)

Equivalent bond distances				Equivalent bond angles	
Atoms	Distance (Å)	Atoms	Distance (Å)	Angle	Deg. (°)
AsS_3H_3 molecule					
Direct bonded distances				∠ *S–As–S*	
As1–S2″	2.2540	As1–S4″	2.2561	∠ S4″–As1–S2″	101.939
As1–S3″	2.2515			∠ S4″–As1–S3″	92.673
Non-bonded distances				∠ S2″–As1–S3″	102.941
S2″–S3″	3.5246	S3″–S4″	3.2608		
S2″–S4″	3.5035				
$As_3S_3H_3$ molecule					
Direct bonded distances				∠ *As–As–As*	
As2–As3	2.4500	As3–As4	2.4589	∠ As3–As2–As4	59.931
As2–As4	2.4728	As3–S2′	2.2724	∠ As2–As3–As4	60.496
As2–S1′	2.2600	As4–S3′	2.2631	∠ As2–As4–As3	59.573
Non-bonded distances				∠ *S–As–As*	
As2–S2′	3.4745	As4–S1′	3.7033	∠ S1′–As2–As3	99.979
As2–S3′	3.7687	As4–S2′	3.5417	∠ S1′–As2–As4	102.882
				∠ S2′–As3–As2	94.668
As3–S1′	3.6095			∠ S2′–As3–As4	96.853
As3–S3′	3.5565			∠ S3′–As4–As2	105.370
				∠ S3′–As4–As3	97.649

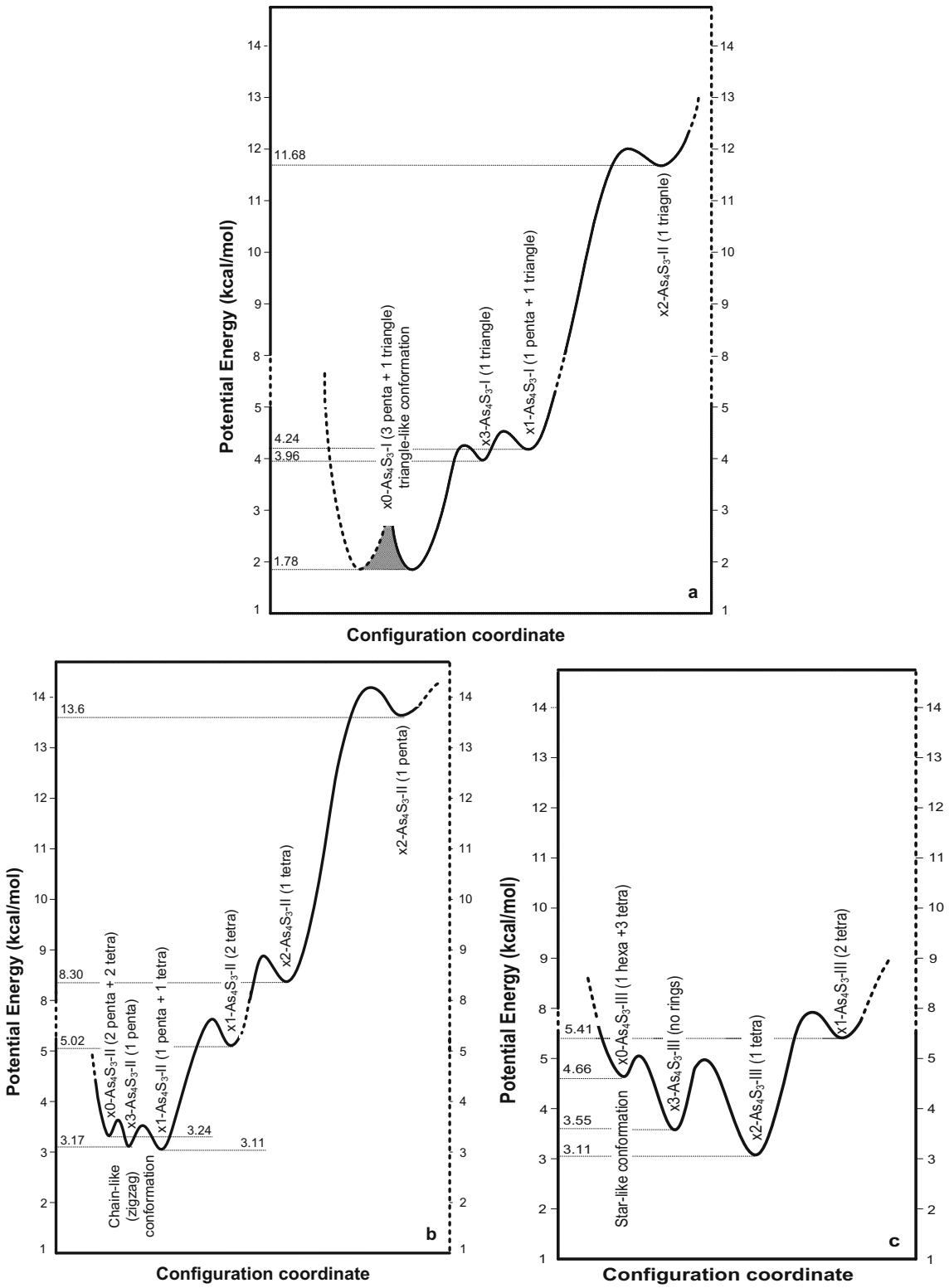

Fig. 6 Potential energy landscapes showing diversity of amorphizing network-forming states originated from As_4S_3 cage-like molecules in different conformations: *triangle*-like (**a**), *chain*-like or *zig-zag* (**b**), and *star*-like (**c**). The double-well presentation of ground state for *triangle*-like As_4S_3-I molecule corresponds to low- and high-temperature modifications of tetra-arsenic trisulphide after Whitfield [12, 13]. The settle-points corresponding to network clusters derived by *x*-fold bond-breaking (keeping small rings, such as triangles/tetragons/pentagons/hexagons nominated in parenthesis) are denoted with respective forming energies E_f at the left axis

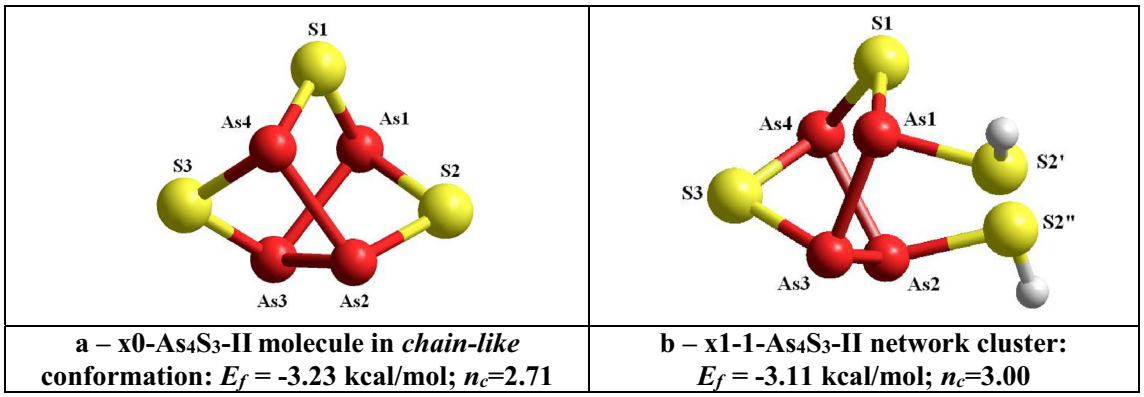

a – x0-As_4S_3-II molecule in *chain-like* conformation: E_f = -3.23 kcal/mol; n_c=2.71

b – x1-1-As_4S_3-II network cluster: E_f = -3.11 kcal/mol; n_c=3.00

Fig. 7 Geometrically-optimized configuration of As_4S_3 cage molecule in *chain-like* conformation × 0-As_4S_3-II (**a**) and its most favorable network derivative × 1–1-As_4S_3-II formed from prototype $As_4S_4H_2$ molecule by single × 1-break in S2 position (**b**). The terminated H atoms are grey colored, S and As atoms are yellow- and red-depicted, and inter-cluster bonds are stick-denoted

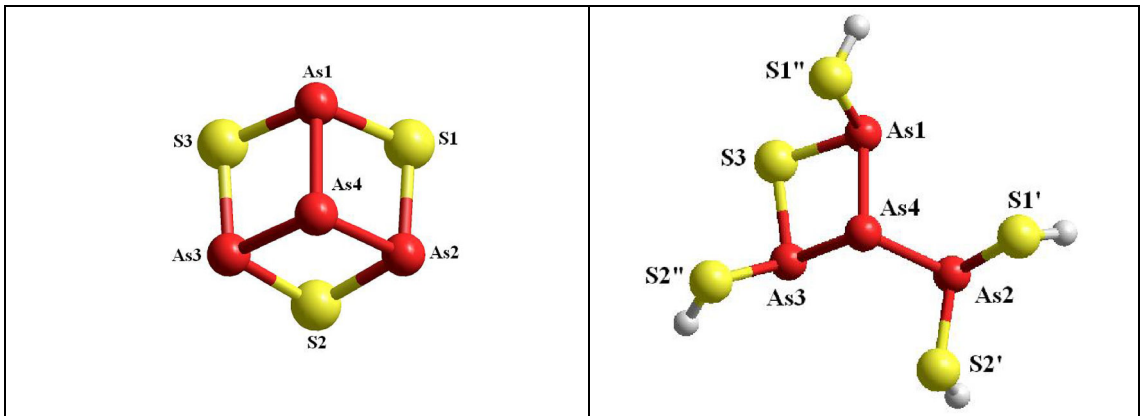

a – x0-As_4S_3-III molecule in star-*like* conformation: E_f = -4.66 kcal/mol; n_c=2.86

b – x2-As_4S_3-III network cluster: E_f = -3.11 kcal/mol; n_c=3.14

Fig. 8 Geometrically-optimized configuration of As_4S_3 cage molecule in *star-like* conformation × 0-As_4S_3-III (**a**) and its most favorable network derivative × 2-As_4S_3-III formed from prototype $As_4S_5H_4$ molecule by double × 2-break in S1 and S2 positions (**b**). The terminated H atoms are grey colored, S and As atoms are yellow- and red-depicted, and inter-cluster bonds are stick-denoted

Competitive Amorphization Scenarios in Nanostructured As_4S_4-As_4S_3 Arsenicals

Recent calorimetric heat-capacity studies of nanoamorphization processes in As_xS_{100-x} arsenicals driven by external influences such as nanomilling testify that amorphous phase generated within As_4S_4–As_4S_3 domain ($2.50 < Z < 2.57$) is close to initial melt-quenched arsenical [20, 21, 40]. This fact assuredly serves as main argumentation on the appeared amorphous phase as mixture of network-forming derivatives originated from realgar As_4S_4-type and dimorphite As_4S_3-type molecules. Alternatively, this process can be classified as *nanomilling-driven amorphization* of melt-quenched alloy [19], in contrast to amorphization associated with decomposition of nanostructured phases occurring in these arsenicals enriched on plastic-crystalline β-As_4S_3 phase [21]. Noteworthy, in respect to temperature-modulated DSC TOPEM® measurements [20, 39], amorphous nanophase generated in these arsenicals possesses double-T_g relaxation, having high-temperature glass-transition mid-point T_{g1} close to that of melt-quenched As_2S_3 alloy and low-temperature glass-transition mid-point T_{g2} near solidus of metastable melting in the respective over-stoichiometric arsenical.

Having in mind this specificity of calorimetric events in As_xS_{100-x} alloys, let's clarify diversity of amorphization scenarios realized in these arsenicals along As_4S_4–As_4S_3 cut-line.

In realgar As_4S_4-type arsenicals with × 0-β-As_4S_4 molecular cluster-precursor (see Fig. 1a), most energetically favorable network-forming amorphizing cluster × 1-β-As_4S_4 can be derived from $As_4S_5H_2$ molecular precursor by single-break in one of S atom positions as illustrated in

Fig. 1b. This amorphization path I from molecular under-constrained arrangement (n_c = 2.875) to network-forming optimally-constrained arrangement (n_c = 3.00) keeping two pentagons is realized with the lowest inter-well barrier of ΔE_f = 0.71 kcal/mol (Fig. 9), thus being basic one for amorphizing As_4S_4-type arsenicals. Competitively, amorphization path II from × 0-β-As_4S_4 molecular precursor to over-constrained (n_c = 3.25) triple-broken derivative (viz. chain-type × 3-β-As_4S_4 cluster) or, alternatively, but with smaller probability, to quadruple-broken derivative (viz. × 4-β-As_4S_4 or $As_2S_{4/2}$ cluster) can be realized in this arsenical with barrier of ΔE_f = 1.14 kcal/mol. Whichever the case, these network-forming clusters (× 1-β-As_4S_4,- × 3-β-As_4S_4 or × 4-β-As_4S_4) are over-stoichiometric ones (Z = 2.50) contributing rather to network modes with low-temperature T_{g2} temperature near solidus of metastable melting in As_4S_4 alloy.

The only variant on phase-decomposed amorphous substance which can be derived from As_4S_4-type alloys appears due to adjacent (neighboring) arrangement of both As–As bonds in pararealgar p-As_4S_4 structure (Fig. 3). Network decomposition occurs from p-As_4S_4 cage-like molecule (Fig. 3a) owing to × 4-break in all S atom positions resulting in × 4-p-As_4S_4 cluster, separating matrix on two sub-networks composed of optimally-constrained $AsS_{3/2}$ pyramids (n_c = 3.00, Z = 2.40) and over-constrained $As_3S_{5/2}$ chains (n_c = 3.36, Z = 2.55) with low barrier of molecular-to-network transition approaching 0.62 kcal/mol, as depicted by amorphization pathway III on Fig. 9. Thus, the amorphous phase generated in this case possesses double-T_g relaxation with high-temperature T_{g1} close to glass-transition mid-point of g-As_2S_3 (∼ 208 °C [39]) and low-temperature T_{g2} near glass-transition mid-point corresponding to solidus of metastable melting of over-stoichiometric $As_{55}S_{45}$ (∼ 130 °C as determined by Hruby [1]). Realistically, such transformations in As_4S_4-type arsenicals are possible just from so-called χ-phase As_4S_4 considered as intermediate precursor of pararealgar p-As_4S_4 phase in light-induced alteration from α/β-As_4S_4 phases [42, 44–46]. This χ-phase As_4S_4 was indeed identified in arsenic monosulphide employing the Raman scattering spectroscopy [20].

From the other side, in dimorphite α/β-As_4S_3-type arsenicals, amorphization can be realized only from As_4S_3 molecules possessing *triangle-like* conformation of neighboring As-As bonds (see Fig. 5a). The most favorable amorphization path IV for this × 0-As_4S_3-I molecule with ΔE_f = 2.18 kcal/mol is connected with matrix decomposition in two optimally-constrained sub-networks (n_c = 3.00) depicted on Fig. 5c, these being composed of $AsS_{3/2}$ pyramids (Z = 2.40) and $As_3S_{3/2}$ clusters (Z = 2.67) keeping three neighboring homonuclear As-As bonds in triangle-like geometry. The latter are responsible for sharp 275 cm^{-1} band ascribed to symmetric-stretch breathing mode

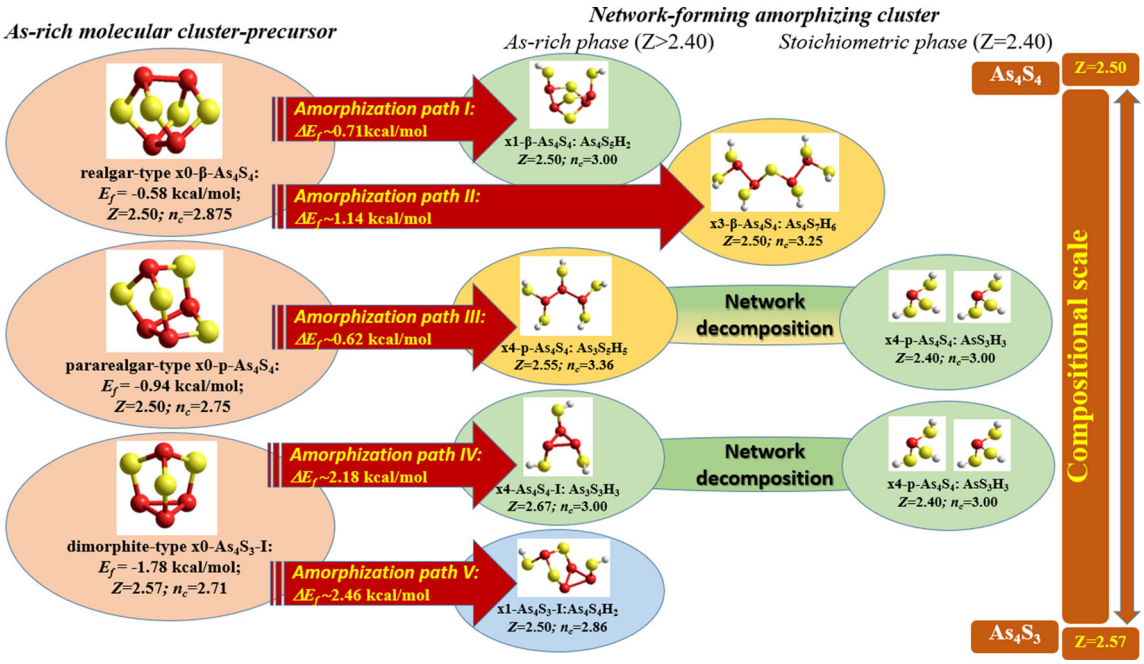

Fig. 9 Competitive amorphization scenarios in nanostructured As_4S_4-As_4S_3 arsenicals driven from boundary compositions of As-rich molecular precursors As_4S_4 and As_4S_3. The molecular precursors of most favorable network-forming clusters are also depicted. The optimally-constrained clusters with n_c = 3.00 are inserted in green boxes, while orange and blue colors are used respectively for over-constrained (n_c > 3.00) and under-constrained clusters (n_c < 3.00). In the cluster marking, terminated H atoms are grey colored, S and As atoms are yellow- and red-colored, and inter-cluster covalent bonds are denoted by respectively-colored sticks

of the basal As_3-rings in the Raman spectra of As_4S_3-type alloys [14, 17, 18, 20, 21, 28]. Thereby, in the current case, the amorphizing substance also demonstrates strong glass-forming ability due to optimally-constrained topology of covalent backbone ($n_c = 3.00$), possessing double-T_g relaxation with distinguishable glass-transition mid-points T_{g1} and T_{g2} as for × 4-p-As_4S_4 clusters derived from pararealgar p-As_4S_4 molecule.

This amorphization path IV dominates in dimorphite As_4S_3-type arsenicals (see Fig. 9), the only competitive amorphization path V being related to incomplete destroying of As_4S_3-I molecule due to single × 1-break stabilizing under-constrained matrix ($n_c = 2.86$) with neighboring small rings in triangle and pentagon configurations (as shown in Fig. 5b). This variant is to be considered rather as defective in view of higher molecular-to-network barrier $\Delta E_f = 2.46$ kcal/mol.

Thus, nanoamorphization in As_4S_4-As_4S_3 arsenicals dominates by clear tendency towards optimally-constrained structural network with $n_c = 3.00$ stabilized via pathways I, III and IV (see Fig. 9), respective molecular-to-network transitions being accompanied by arsenical decomposition on stoichiometric ($Z = 2.40$) and over-stoichiometric ($Z > 2.40$) sub-networks via path III and IV. Competitive contribution of these amorphization scenarios is defined preferentially by arsenical composition, where higher barriers of molecular-to-network transition in dimorphite-type As_4S_3 arsenicals ($\Delta E_f > 2$ kcal/mol) allow As_4S_4-As_4S_3 alloys nominated as higher-crystalline ones, in full respect to terminology of Hruby [1].

The unified potential energy landscape showing diversity of molecular-to-network amorphization scenarios in the studied nanostructured arsenicals realized for boundary As_4S_4 and As_4S_3 components is shown on Fig. 10.

Under nanostructurization due to high-efficient external influence such as nanomilling, the role of As_4S_4-type arsenicals is mainly revealed through amorphization transitions from under-constrained realgar-type × 0-β-As_4S_4 molecule ($n_c = 2.875$) supplemented by transitions from under-constrained pararealgar-type × 0-p-As_4S_4 ones ($n_c = 2.75$). The former dominates by appearance of network-forming optimally-constrained × 1-β-As_4S_4 clusters (having $n_c = 3.00$ and molecular-to-network barrier approaching $\Delta E_f = 0.71$ kcal/mol) along with over-constrained × 3-β-As_4S_4 clusters (having $n_c = 3.25$ and $\Delta E_f = 1.14$ kcal/mol). The latter dominates mainly by transformation towards × 4-p-As_4S_4 clusters separating the arsenical matrix on two sub-networks composed of stoichiometric optimally-constrained $AsS_{3/2}$ trigonal pyramids ($Z = 2.40$, $n_c = 3.00$) and As-rich non-stoichiometric over-constrained $As_3S_{5/2}$ chains ($Z = 2.55$, $n_c = 3.36$). In this case, the degree of network decomposition in nanoarsenical (and, respectively, the parameters of double-T_g relaxation) is defined by completeness of preliminary alteration from α/β-As_4S_4 phase to metastable pararealgar p-As_4S_3 phase through its intermediate precursor (such as χ-phase As_4S_4).

In As_4S_3-type arsenicals, main amorphization scenario is connected with transition from under-constrained dimorphite-type × 0-As_4S_3-I molecules ($Z = 2.57$, $n_c = 2.71$) possessing *triangle-like* configuration in the nearest arrangement of three neighboring homonuclear As-As bonds (as depicted in Fig. 5a) to their triple-broken × 3-As_4S_3-I derivatives. The respective structural transformations separate arsenical matrix on two optimally-constrained sub-networks (both having $n_c = 3.00$) composed of $AsS_{3/2}$ pyramids ($Z = 2.40$) and over-stoichiometric As-rich $As_3S_{3/2}$ clusters ($Z = 2.67$) keeping the basal As_3-rings. This amorphization scenario can be only slightly disturbed (if any) by incomplete destroying of As_4S_3-I molecules owing to single × 1-breaking in one of S atom positions, thus stabilizing intrinsically uniform but rather under-constrained (in view of $n_c = 2.86$) network with cluster-forming energy approacging $E_f = -4.24$ kcal/mol (see Fig. 9).

Conclusions

Complete hierarchy of network-forming amorphization scenarios in As_xS_{100-x} nanoarsenicals within As_4S_4-As_4S_3 cut-Sect. ($50 \le x \le 57$) is reconstructed employing materials-computational approach based on *ab-initio* quantum-chemical modeling code (CINCA).

Under nanostructurization caused by external influence such as high-energy mechanical milling, complicated inter-crystalline phase transformations towards nanoscopic high-temperature β-As_4S_4 polymorph accompanied by appearance of compositionally-invariant covalent-network amorphous phase are activated in these alloys. General amorphization trend under nanomilling obeys tending from molecular cage-like structures to optimally-constrained covalent networks which are isocompositional to the parent alloy. Optimal topological constitution of amorphous phase generated in nanoarsenicals is ensured by diversity of respective small-ring configurations incorporated in their covalent networks. Contribution of network-forming amorphization pathways in As_4S_4-As_4S_3 nanoarsenicals is defined by their chemistry with higher molecular-to-network transition barriers proper for As_4S_3-rich alloys (more than ~ 2 kcal/mol). The generated amorphous phase is intrinsically decomposed, possessing double glass-transition temperature T_g relaxation due to stoichiometric (x = 40) and non-stoichiometric (x > 40) sub-networks, which are respectively built of $AsS_{3/2}$ pyramids and As-rich entities keeping two separated As-As bonds derived from realgar-type molecules, two neighboring As-As bonds

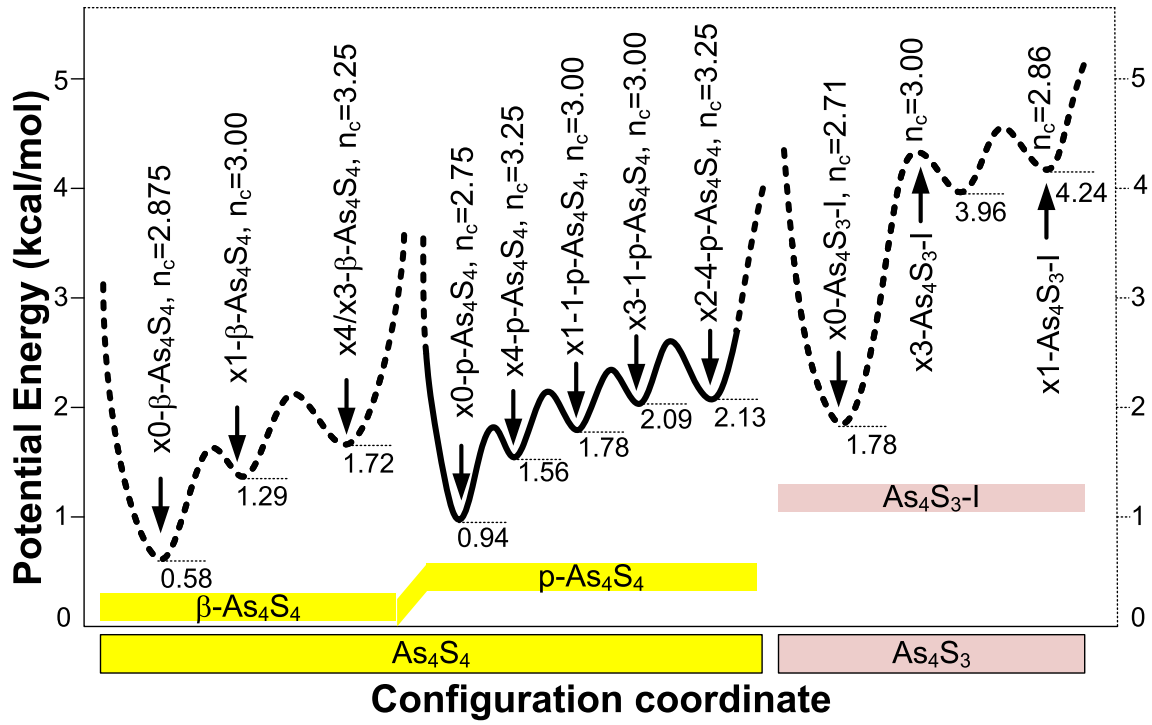

Fig. 10 Unified potential energy landscape showing diversity of main molecular-to-network amorphization transitions in nanostructured As_4S_4-As_4S_3 arsenicals, restricted for boundary As_4S_4 (left) and As_4S_3 (right) compositions. The calculated cluster-forming energies (E_f) are right-side denoted near energy wells corresponding to molecular clusters and their most favorable network derivatives pointed out by arrows (the atom-averaged topological constraints n_c are indicated)

derived from pararealgar-type molecules and/or three neighboring As-As bonds in triangle-like geometry derived from dimorphite-type molecules. Compositional invariance of nanomilling-derived amorphous phase in As_xS_{100-x} arsenicals within As_4S_4-As_4S_3 cut-section is ensured by network-forming clusters generated in a growing sequence with average coordination number Z: ($As_2S_{4/2}$, $Z = 2.50$) – ($As_3S_{5/2}$, $Z = 2.55$) – ($As_3S_{3/2}$, $Z = 2.67$). Full diversity of molecular-to-network amorphization pathways in the studied As_4S_4-As_4S_3 nanoarsenicals is specified on unified potential energy landscape for boundary As_4S_4 and As_4S_3 components.

Acknowledgements The paper is part of scientific research performed within the project No 0119U100357, subject of Scientific Program funded by Ministry of Education and Science of Ukraine (2019-2022).

Data Availability The raw/processed data required to reproduce these findings cannot be shared at this time due to technical or time limitations.

Declarations

Conflict of interest The authors declare that they have no conflict of interest.

References

1. A. Hruby and J. Non-Cryst (1978). *Solids* **28**, 139.
2. Z. U. Borisova, *Glassy Semiconductors*. (Plenum Press, New York, 1981), pp. 1–505.
3. A. Feltz, *Amorphous Inorganic Materials and Glasses*. (VCH Publ, New York, 1993), pp. 1–446.
4. A. L. Emelina, A. S. Alikhanian, A. V. Steblevskii, and E. N. Kolosov (2007). *Inorg. Mater.* **43**, 95.
5. J.-L. Adam, X. Zhang (Eds.), *Chalcogenide glasses: Preparation, properties and applications*. (Woodhead Publ. Ser. in Electronics and Optical Mater., Philadelphia-New Delhi, 2013), pp. 1–716.
6. O. Shpotyuk and M. Hyla (2017). *J. Optoelectron. Adv. Mater.* **19**, 48.
7. P. J. Dilda and P. J. Hogg (2007). *Cancer Treat. Rev.* **33**, 542.
8. P. Bonazzi and L. Bindi (2008). *Z. Ktistallogr.* **223**, 132.
9. O. Shpotyuk, P. Demchenko, Y. Shpotyuk, Z. Bujňáková, P. Baláž, and J. Non-Cryst (2019). *Solids* **505**, 347.

10. O. Shpotyuk, P. Baláž, Z. Bujňáková, A. Ingram, P. Demchenko, and Y. Shpotyuk (2018). *J. Mater. Sci.* **53**, 13464.
11. P. Chen, C. Holbrook, P. Boolchand, D. G. Georgiev, K. A. Jackson, and M. Micoulaut (2008). *Phys. Rev. B* **78**, 224208.
12. H.J. Whitfield (1970). *J. Chem. Soc. A*, 1800.
13. H.J. Whitfield (1973). *J. Chem. Soc. Dalton*, 1737.
14. A. C. Wright, B. G. Aitken, G. Cuello, R. Haworth, R. N. Sinclar, J. R. Stewart, J. W. Taylor, and J. Non-Cryst (2011). *Solids* **357**, 2502.
15. T. N. Chattopadhyay, E. Gmelin, and H. G. von Schnering (1983). *Phys. Stat. Sol. A* **76**, 543.
16. R. Blachnik and U. Wickel (1984). *Thermochim. Acta* **81**, 185.
17. B. G. Aitken and J. Non-Cryst (2004). *Solids* **345–346**, 1.
18. S. Soyer-Uzun, S. Sen, B.G. Aitken (2009). *J. Phys. Chem. C* **113**, 6231.
19. O. Shpotyuk, P. Demchenko, Y. Shpotyuk, Z. Bujňáková, P. Baláž, M. Hyla, and V. Boyko (2019). *Mater Today Commun* **21**, 100679.
20. O. Shpotyuk, P. Demchenko, Y. Shpotyuk, S. Kozyukhin, A. Kovalskiy, A. Kozdras, Z. Lukáčová Bujňáková, and P. Baláž (2020). *J. Non-Cryst. Solids* **539**, 120086.
21. O. Shpotyuk, S. Kozyukhin, P. Demchenko, Y. Shpotyuk, A. Kozdras, M. Vlcek, A. Kovalskiy, Z. Lukáčová Bujňáková, P. Baláž, V. Mitsa, and M. Veres (2020). *J. Non-Cryst. Solids* **549**, 120339.
22. O. Shpotyuk, M. Hyla, V. Boyko, Y. Shpotyuk, and V. Balitska (2020). *Appl. Nanosci.* **10**, 4689.
23. O. Shpotyuk, M. Hyla, and V. Boyko (2013). *J. Optoelectron. Adv. Mater.* **15**, 1429.
24. O. Shpotyuk, M. Hyla, and V. Boyko (2015). *Comput. Mater. Sci.* **110**, 144.
25. W. J. Hehre, R. F. Stewart, and J. A. Pople (1969). *J. Chem. Phys.* **51**, 2657.
26. A. D. McLean and G. S. Chandler (1980). *J. Chem. Phys.* **72**, 5639.
27. K. Jackson (2000). *Phys Stat Solidi B* **217**, 293.
28. R. Holomb, M. Veres, and V. Mitsa (2009). *J. Optoelectron. Adv. Mater.* **11**, 917.
29. O. Shpotyuk, A. Ingram, and P. Demchenko (2015). *J. Phys. Chem. Solids* **79**, 49.
30. J. C. Phillips and J. Non-Cryst (1979). *Solids* **34**, 153.
31. M. F. Thorpe and J. Non-Cryst (1983). *Solids* **57**, 355.
32. M. F. Thorpe and J. Non-Cryst (1995). *Solids* **182**, 135.
33. T. Ito, N. Morimoto, and R. Sadanaga (1952). *Acta Cryst.* **5**, 775.
34. D. J. E. Mullen and W. Nowacki (1972). *Zeit. Krist.* **136**, 48.
35. E. J. Porter and G. M. Sheldrick (1972). *J. Chem. Soc. Dalton Trans.* **13**, 1347.
36. L. Bindi, G. Pratesi, M. Muniz-Miranda, M. Zoppi, L. Chelazzi, G. O. Lepore, and S. Menchetti (2015). *Mineral. Mag.* **79**, 121.
37. P. Baláž, W. S. Choi, and E. Dutková (2007). *J. Phys. Chem. Solids* **68**, 1178.
38. P. Baláž, M. Baláž, O. Shpotyuk, P. Demchenko, M. Vlček, M. Shopska, J. Briančin, Z. Bujňáková, Ya. . Shpotyuk, B. Selepová, and L. Balážová (2017). *J. Mater. Sci.* **52**, 1747.
39. O. Shpotyuk, Z. Bujňáková, M. J. Sayagués, P. Baláž, A. Ingram, Ya. . Shpotyuk, and P. Demchenko (2017). *Mater. Charact.* **132**, 303.
40. O. Shpotyuk, A. Kozdras, P. Baláž, Z. Bujňáková, and Ya. . Shpotyuk (2019). *J. Therm. Anal. Calorim.* **135**, 2945.
41. P. Bonazzi, S. Menchetii, and G. Pratesi (1995). *Am. Mineral.* **80**, 400.
42. P. Bonazzi, S. Manchetti, G. Pratesi, M. Muniz-Miranda, and G. Sbrana (1996). *Am. Mineralogist* **81**, 874.
43. A. Kyono (2013). *Phys. Chem. Minerals* **40**, 717.
44. D. L. Douglass, C. Shing, and G. Wang (1992). *Am. Mineralogist* **77**, 1266.
45. K. Trentelman and L. Stodulski (1996). *Anal. Chem.* **68**, 1755.
46. M. Muniz-Miranda, G. Sbrana, P. Bonazzi, S. Menchetti, and G. Pratesi (1996). *Spectrochim. Acta A* **52**, 1391.

Authors and Affiliations

Oleh Shpotyuk[1,2] · Malgorzata Hyla[1] · Yaroslav Shpotyuk[3,4] · Valentina Balitska[5] · Andrzej Kozdras[6] · Vitaliy Boyko[2]

✉ Oleh Shpotyuk
o.shpotyuk@ujd.edu.pl; olehshpotyuk@yahoo.com

Yaroslav Shpotyuk
yashpotyuk@gmail.com

Valentina Balitska
v.balitska@yahoo.com

Andrzej Kozdras
akozdras@po.opole.pl

[1] Faculty of Science and Technology, Jan Dlugosz University in Czestochowa, 13/15, al. Armii Krajowej, 42200 Czestochowa, Poland

[2] Department of Optical Glass and Ceramics, Vlokh Institute of Physical Optics, 23, Dragomanova st, Lviv 79005, Ukraine

[3] Department of Sensor and Semiconductor Electronics, Ivan Franko National University of Lviv, 107, Tarnavskoho str, Lviv 79017, Ukraine

[4] Institute of Physics, University of Rzeszow, 1, Pigonia st., 35959 Rzeszow, Poland

[5] Department of Physics and Chemistry of Combustion, Lviv State University of Life Safety, 35, Kleparivska str, Lviv 79007, Ukraine

[6] Opole University of Technology, 75, Ozimska str, 45370 Opole, Poland